Imperial College London
Robert Steiner MR Unit
Hammersmith Hospital

Parallel Transmission MRI

Jason Filos

November 2008

Supervised by
Professor Jo Hajnal and Dr David Larkman

Imperial College
London

Submitted in part fulfilment of the requirements for the degree of
the Diploma of Imperial College London

Abstract

Following the development of parallel imaging within the MR community, focus has been drawn towards the research area known as parallel transmission. Based on the back of the advancements achieved with parallel receive, parallel transmission can be used to improve RF excitation by shortening the pulse duration and reducing the occurring specific absorption rate. In this project we develop a methodology aimed at reducing problems induced by the non linear behaviour of the main magnetic field (B_0-field) through controlled alteration of the transmit coil fields (B_1-field). The feasibility of this method is shown using computer simulation based on the specifications of a multi-channel capable clinical scanner. Additionally a software controlled hardware add-on system, to upgrade a conventional single-channel clinical scanner to multi-channel capabilities, is outlined in this project.

Contents

List of Tables

List of Figures

1. Introduction

Magnetic Resonance Imaging (MRI) is a tomographic imaging technique that produces images of internal physical and chemical characteristics of an object from externally measured nuclear magnetic resonance (NMR) signals [1].

1.1. MRI Basics

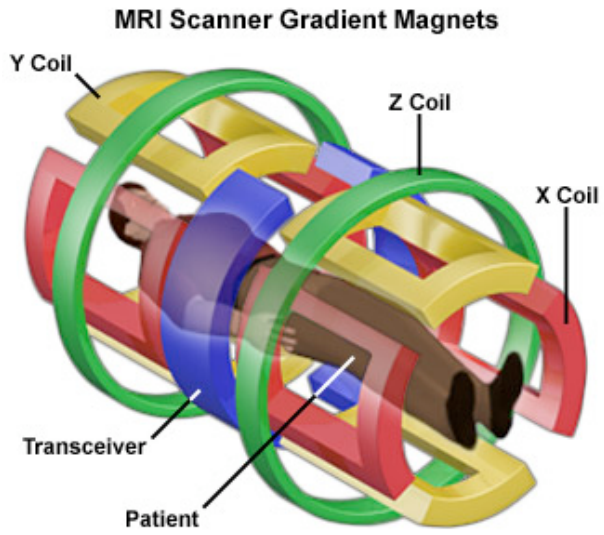

Figure 1.1.: MR Scanner Gradient Coils (Source: http://www.magnet.fsu.edu).

An MRI scanner is an important clinical tool and from a system perspective consists of three main hardware components: a main magnet, a magnetic field gradient system, and a radiofrequency (RF) system. The primary function of the main magnet is to generate a strong uniform static field; this field is referred to as the B_0 field, for polarization of nuclear spins in an object. The magnetic field gradient system normally consists of three orthogonal gradient coils (Figure 1.1). These coils are designed to produce time-varying magnetic fields of controlled spatial non-uniformity; they are used to impose magnetic fields that vary in amplitude linearly with spatial distance. The gradient system is an important component of the MRI scanner because it is essential for signal localization. Finally the RF system consists of a transmitter coil that is capable of generating a rotating magnetic field, this field is referred to as the B_1 field, for excitation of a spin system, and a receiver coil that converts a precessing magnetization into an electrical signal. The transmission and reception of the electrical signal is not necessarily handled by two distinct coils, a single transceiver coil can be employed, although generally a single coil is used for transmission and an array of coils for reception. These coils are usually called RF coils because they resonate at a specific radio frequency,

as required by the spin excitation and signal detection. The specific resonant frequency of the spin system is known as the *Larmor frequency*, which is defined as the angular frequency of nuclear precession:

$$\omega_0 = \gamma B_0, \tag{1.1}$$

where γ is defined as the gyromagnetic ratio. The ^1H nucleus has a γ value of roughly 2.68×10^8 rad/s/Tesla.

The gradient field mentioned in the previous paragraph plays a pivotal role in the spatial localization of the signal. In what is known as spatial encoding by applying the gradients we can make the magnetic field strength, and thus the Larmor frequency, spatially dependent over a selected target area. In this way our representation of frequency can be mapped to space and the spatial distribution of signals can be recovered from a measured time course signal by Fourier Transform. In MRI, acquisition is done in what is referred to as k-space, this is a reciprocal space to the image. Each point in k-space affects every point in the image.

An important aspect of MR imaging is the quality of the image we obtain after a scan. We quantify the image quality according to various criteria such as how much signal there is present with respect to the noise level, also known as the signal-to-noise ratio (SNR) or how corrupted by artefacts the image is. Another important aspect of MR imaging is the resolution of the image, which we aim to maximize. There is a trade-off between the above mentioned measures of image quality and imaging speed and it is therefore desirable to devise techniques which can improve on the resolution and quality of the images while maintaining a respectable imaging speed. Many researchers are seeking for methods to reduce the amount of acquired data without degrading the image quality. There have been numerous proposed concepts to achieve a considerable improvement in imaging speed ranging from pulse sequence design to leaving out redundant data in k-space, the latter of which is often referred to as undersampling k-space information.

When k-space is undersampled, the Nyquist criterion may be violated, and Fourier reconstructions may exhibit aliasing artefacts. Previous methods for reconstructing such data have been proposed. As shown by [2] they fall in three groups: (a) Methods generating artefacts that are incoherent or less visually apparent, at the expense of reduced apparent SNR; (b) Methods exploiting alternative encoding methods, such as parallel imaging, etc.; (c) Methods exploiting either spatial or temporal redundancy or both [3].

Parallel imaging is an imaging technique which relies on a greater number of receiver coils, i.e. the reception of the signal resulting from the excited spin system is captured in parallel from an array of coils. Since each coil is more sensitive to spin packets in its spatial proximity, we can make use of this information in a number of ways. As will be shown this yields many potential advantages and we can use parallel imaging techniques to address the pitfalls outlined in the previous paragraph, namely improving image quality under certain conditions.

As outlined by [4] following the development of parallel imaging, interest has been drawn towards the topic known as parallel transmission, which describes the use of multiple RF transmit coils. Parallel transmission can be applied to improve RF excitation, in particular, multidimensional spatially selective RF excitation, by shortening the pulse duration and overall minimizing the occurring specific absorption rate (SAR). One potential major application might be the compensation of patient-induced B_1 inhomogeneities (caused by the magnetic susceptibility of tissue), particularly at high field strengths.

The purpose of this project is to find out to what degree we can account for B_0 induced problems with B_1 control. We will use an exemplar of a standard slice selective excitation performed in a non-uniform B_0 field which results in a bent slice profile. We will focus on a series of simulations which tackle the above problem and follow on with a comparison of two proposed methods depicting how a straight slice profile can be obtained in a non-uniform B_0 field. It will be shown that each of the methods requires different degrees of control over the B_1 field.

2. Background

2.1. Transmission in Standard MRI

In standard single channel MRI the transmission (Tx) process is conducted in the following way. The RF system generates a magnetic field which excites a spin system; this in turn generates a signal, which can be measured. The generated signal can be localized using the gradient system. The phase and amplitude of the signal can be controlled by the transmitter. When using a higher number of transmit coils, the transmitted field is the vector sum of all the fields. The flexibility of a multiple Tx system is thus exemplified by the fact that it can globally and locally alter the Tx field.

2.2. Parallel Imaging

Parallel receive has been shown to yield many benefits when compared to a single element receive architecture [5]. Parallel Transmission (PTx) however is a fairly novel approach in the scientific community. It holds many potential advantages over a single coil transmission scheme. In parallel transmission systems using a higher number of local coils can be used to spatially sculpt the B_1 field using standard sequences. According to [6] it is therefore possible to account for B_1 field inhomogeneities which are induced by the interaction between the patient with the main magnetic field for example. This technique referred to as RF-Shimming might prove important for clinical applications at high field strengths ($\geq$ 3T). Accounting for these B_1 inhomogeneities is one of the major applications of PTx. Additionally parallel transmission is able to shorten spatially selective RF pulses in two or three dimensions, or to minimize the occurring SAR. By [7] it is shown that localised excitation takes a very long time using a single element coil. The idea of using parallel imaging to shorten the acquisition time by the simultaneous use of multiple receive coils can be adapted for the parallel transmission of a spatially-selective multidimensional RF pulse. As in data acquisition, a multidimensional RF pulse follows a certain k-space trajectory. Shortening this trajectory shortens the pulse duration. The use of multiple transmit coils, each with its own time-dependent waveform and spatial sensitivity, can compensate for the missing parts of the excitation k-space. This results in a maintained spatial definition of the

pulse profile, while its duration is reduced. According to [8] the maximum speedup factor can be approximately equal to the number of coil elements used.

2.3. Tackling B_0 Problems with B_1 Control

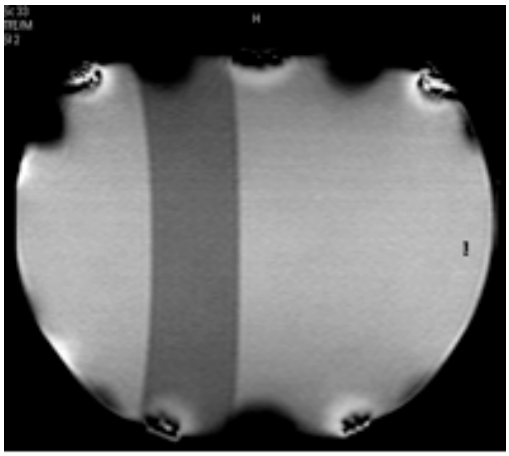

Figure 2.1.: Bent rest slab in large oil phantom at 3T (FOV 40cm x 40cm with fold-over on edges due to size of phantom being greater than FOV).

There are a variety of inconsistencies which are apparent in various different clinical applications. One such example is that slices appear to be bent the further the object is placed away from the iso-centre of the magnet. As depicted in figure 2.1 it can be seen that a rest slab placed away from centre does not appear straight. The origin of this problem lies in the spatial variation (or inhomogeneity) of the main magnetic field. This is a problem which could be possibly alleviated in a PTx system by inducing a change in the local or global transmit field (B_1). Using PTx we have enough degrees of freedom to excite different parts of the body using different parameters, such as individual phase and amplitude modulation, to possibly alleviate this problem. We will consider two methods in the following section. They are aimed at taking into account the homogeneities and distortions resulting inside our imaging area and accounting for any effects induced in the resulting excitation. In the subsequent section these methods will then be evaluated through experimental simulation.

3. Theory

This chapter outlines the methods behind the simulation of the slice-correction algorithm. Starting with a formalism for the RF pulse design of a slice selective excitation in the small tip angle approximation, we will lay the groundwork for two methods depicting how a straight slice profile can be obtained under conditions of B_0 inhomogeneity. These two methods differ in the way they control or sculpt the B_1 field. It will be shown that the first method introduced allows for more degrees of control of the B_1 field than the second method.

3.1. RF Pulse Design for Slice Selection in the Small Tip Angle Approximation

We can formally define slice selection as follows.
Consider generating a rectangular slice profile. This implies that a sinc pulse will be applied in the time domain. The effective B_1 is then given by

$$\hat{B}_1^e(t) = B_1 \mathrm{sinc}\left[\pi \Delta \mathrm{f}(\mathrm{t} - \frac{\tau_\mathrm{p}}{2})\right] \prod\left(\frac{\mathrm{t} - \tau_\mathrm{p}/2}{\tau_\mathrm{p}}\right), \tag{3.1}$$

where τ_p is the total pulse duration.
Since the total pulse duration is not known a priori we need to use an approximation by setting t_L as the time until the first zero crossing of the sinc function. The flip angle θ is related to the B_1 field by

$$\Delta\theta = \gamma \cdot B_1 \cdot \tau, \tag{3.2}$$

where τ is the time associated with the zero-crossing of the sinc function. Hence by setting $\sin(\pi \Delta f(t_L - \frac{\tau_p}{2})) = 0$, we obtain $(t_L - \frac{1}{\Delta f}) \cdot 2 = \tau_p$. Additionally, the thickness of the excited slice associated with this sinc pulse is given by

$$TH = \frac{BW_{rf}}{\gamma G_{0,z}} = \frac{2\pi}{\gamma G_{0,z} \tau_p}. \tag{3.3}$$

3.2. Spatial Domain Method

The following method presented is based on a concept introduced by [9]. It presents an approach for RF pulse design in parallel excitation which allows the use of arbitrary k-space trajectories, closely related to transmit SENSE, but formulated in the spatial domain. It designs the excitation k-space for a given object and set of coils; the choice of k-space trajectory and set of coils can be arbitrarily defined. It will later be shown that for our purposes this method is implemented using a single line of k-space, or a single "spoke" in the direction of slice excitation.

By [8] the multicoil iterative pulse design method is based on the minimization of a quadratic cost function that consists of an excitation error term, which quantifies excitation error in the spatial domain. It is important to note, that in this method the main field inhomogeneity can be incorporated in the design. This means that we can estimate a set of optimal pulses for each coil, which take the non-linearity of the main magnetic field into account. If we evaluate this non-linearity by means of a B_0-map and feed it into the system, we can account for off-resonance effects inside the Field Of View (FOV).
The formulation is based on the small-tip-angle approximation, which means that the transverse plane excitation pattern produced by a single coil can be approximated by the Fourier integral of an excitation k-space trajectory, weighted by a complex RF pulse and spatially weighted by the coils complex transmit sensitivity $s(\mathbf{x})$:

$$m(\mathbf{x}) = i\gamma m_0 s(\mathbf{x}) \int_0^T b(t) e^{i\gamma \Delta B_0(\mathbf{x})(t-T)} e^{i\mathbf{x}\mathbf{k}(t)} dt, \tag{3.4}$$

where $\mathbf{k}(t) = \begin{bmatrix} k_x(t) & k_y(t) & k_z(t) \end{bmatrix}$, $b(t)$ is the complex RF pulse, γ the gyromagnetic ratio, m_0 the equilibrium magnetization magnitude, T the pulse length, and where $e^{i\gamma \Delta B_0(\mathbf{x})(t-T)}$ represents the phase accrued due to main field inhomogeneity defined by the field map $\Delta B_0(\mathbf{x})$. Because we are dealing in the small tip angle regime it is possible to construct a linear combination of the transmit coils to form an aggregate pattern:

$$m(\mathbf{x}) = i\gamma m_0 \sum_{r=1}^{R} s_r(\mathbf{x}) \int_0^T b_r(t) e^{i\gamma \Delta B_0(\mathbf{x})(t-T)} e^{i\mathbf{x}\mathbf{k}(t)} dt, \tag{3.5}$$

where R represents the number of transmit coils, each with their own sensitivity pattern $s_r(\mathbf{x})$ and unique RF pulse $b_r(t)$. By discretizing time and space this may be written as:

$$\mathbf{m} = \sum_{r=1}^{R} \mathbf{D}_r \cdot \mathbf{A} \cdot \mathbf{b}_r, \tag{3.6}$$

where m is the vector of spatial samples of the aggregate excitation pattern, $\mathbf{D}_r = \mathrm{diag}\{\mathrm{s_r}(\mathbf{x_i})\}$ is a diagonal matrix containing samples of the sensitivity pattern of coil r and $\mathbf{b}_r$ is a vector of RF pulse samples for coil r. The system matrix $\mathbf{A}$ is given by:

$$a_{ij} = i\gamma m_0 \Delta t e^{i\gamma \Delta B_0(\mathbf{x}_i)(t_j - T)} e^{i\mathbf{x}_i \mathbf{k}(t_j)}. \tag{3.7}$$

Equation (3.6) can be rewritten via horizontal concatenation of the matrices $\mathbf{D}_r\mathbf{A}$ and vertical concatenation of the vectors $\mathbf{b}_r$ resulting in:

$$\mathbf{m} = [\mathbf{D}_1\mathbf{A} \cdots \mathbf{D}_R\mathbf{A}] \begin{bmatrix} \mathbf{b}_1 \\ \vdots \\ \mathbf{b}_R \end{bmatrix} = \mathbf{A}_{full} \cdot \mathbf{b}_{full}. \tag{3.8}$$

The RF pulses can then be designed by solving the following minimization problem:

$$\hat{\mathbf{b}}_{full} = \arg\min_{\mathbf{b}_{full}} \left\{ \|\mathbf{A}_{full} \cdot \mathbf{b}_{full} - \mathbf{m}_{des}\|^2 \right\}, \tag{3.9}$$

where the vector m_{des} contains samples of a desired pattern at the spatial locations x_i. An alternative, but related to the spatial domain method presented here, would be the frequency domain approach which solves the problem:

$$\mathbf{p}_{des} = \mathbf{s}_{full} \cdot \mathbf{p}_{full}. \tag{3.10}$$

Note that this formalism can be used to directly tackle the bent slice problem to produce a desired excitation profile in a non uniform magnetic field.

3.3. Extended B_1-Shimming Method

In this section we will present an alternative method to address the problems of poor B_0 homogeneity using a multi-element transmit system. As introduced in the background section of this report, it is possible to tailor B_1 fields using a multitude of transmit coils. The basic idea behind this arises from the fact that the effective B_1 is the superposition of the individual transmit fields B_{1i}:

$$B_1(r,t) = \sum_{i=0}^{R} S_i(r) \cdot B_{1i}(t). \tag{3.11}$$

It is possible to achieve B_1 homogenisation using a standard slice selective RF pulse. In order to do this the amplitude and the phase need to be modulated

independently for each coil:

$$B_1(r,t) = \sum_{i=0}^{R} S_i(r) \cdot a_i \cdot B_1(t). \tag{3.12}$$

This can be solved in a classical least squares way by setting:

$$T(r) = \sum_{i=0}^{R} S_i(r) \cdot a_i, \tag{3.13}$$

resulting in $\mathbf{T} = \mathbf{S} \cdot \mathbf{a}$, where $\mathbf{T}$ is the target field distribution. The solution can be obtained by solving:

$$\mathbf{a} = \arg\min_{\mathbf{a}} \left\{ \|\mathbf{S} \cdot \mathbf{a} - \mathbf{T}\|^2 \right\}. \tag{3.14}$$

Using the above methodology we can improve the transmit B_1 homogeneity by appropriate superposition of the individual transmit fields B_{1i}. Note however that as opposed to the method by Grissom et al., the phase of the transmitted pulse does not vary in time. Thus in order to correct for off-resonance effects manifested as frequency shifts in our excitation, making a slice appear bent, the above concept needs to be extended.

We can relate the flip-angle map to parameters representing the centre-frequency, amplitude and phase via a mapping function $G(b(f, A, \phi))$ and minimize according to:

$$\left\| \mathbf{T}_{des} - \sum_{c=1}^{R} S_c \cdot G(b_c(f_c, A_c, \phi_c)) \right\|_{\min \mathrm{f_c}, \mathrm{A_c}, \phi_\mathrm{c}}. \tag{3.15}$$

For an eight-coil parallel excitation system we thus have a total of twenty-four parameters expressing frequency, amplitude and phase shifts. It is important to note however that this method has less degrees of control over the B_1 field than the spatial domain method. Note that in this formalism only the *global* amplitude and phase of the RF pulse is modulated as opposed to estimating a solution for each point of the pulse as depicted in the spatial domain approach.

4. Methods

In this chapter we will outline how the previously established concepts can be implemented and evaluated by means of a simulation in a computer environment using MATLAB (MathWorks, Inc., Natick, MA). The various components of this simulation are based on an experimental framework which models the main elements of a clinical MRI scanner, such as the main magnetic field and the RF system, along with an optimization routine which attempts to obtain a desired solution given perturbations introduced in the system. Building on the concepts of parallel transmission we will outline an implementation which derives an optimal solution for the RF pulse played out on a set number of transmit coils. Two distinct methods have been outlined previously, and they differ by the parameter space available to control this RF pulse. It will be shown that the method based on the Grissom methodology estimates a solution for each time point of the RF pulse for each coil, thus having more degrees of freedom compared to the extended B_1 shimming method which only modulates the global offset frequency, amplitude and phase of an original excitation RF pulse independently for each coil. The reference system for this simulation is an 8-channel Philips "Multix" scanner, from which real coil data is included in the simulation. A more detailed description of this scanner will be presented alongside an outline of a hardware add-on system, devised for the purposes of this project, which can be used to upgrade an existing single channel scanner to support the parallel transmission concepts established in the previous chapter.

4.1. Slice Selection

Using the definition of slice selection, outlined in the previous chapter, and the Fourier transform, on grounds of the small-tip-angle approximation, it is relatively straightforward to implement a simulation of a slice selective RF pulse. From $\Delta\theta = \gamma \cdot B_1 \cdot \tau$ we can see that by defining the flip angle and the B_1 field we can solve for the time until the first zero crossing, which in turn lets us estimate the total RF pulse duration. This way we can estimate the pulse values and the resulting slice profile. Note that the sampling rate is set to $6\mu s$, according to the specifications of the scanner. The pulse is then additionally smoothed via a

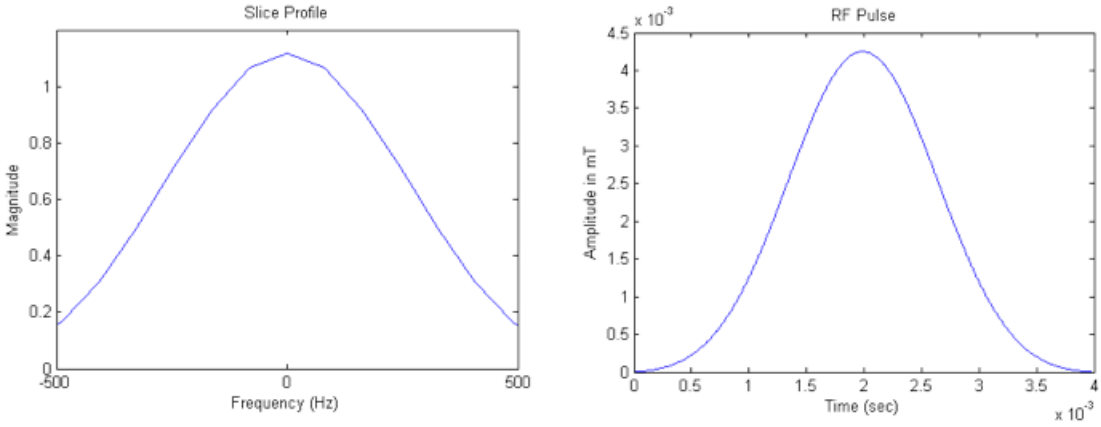

Figure 4.1.: RF pulse and resulting slice profile (BW = $1000Hz$, B_1=$4.25\mu T$, FA=$90°$)

Gaussian windowing function. By taking the Fourier transform of this smoothed pulse we obtain a Gaussian slice profile as shown in figure 4.1.

4.2. Spatial Domain Method

The different steps needed to implement the methodology outlined by Grissom et al. are as follows:

1. Definition of the Field of Excitation (FOX) and excitation k-space trajectory (one "y-spoke" in our example).
2. Definition of the main field inhomogeneity (a Gaussian variation increasing in magnitude as we move away from the center of the FOX).
3. Generation of the target excitation pattern (Using the slice selection routine outlined above).
4. Calculation of the encoding matrix and the complex coil profiles.
5. Estimation of the RF pulse by means of matrix inversion in a least-squares way.

Since the field inhomogeneity is modeled using a Gaussian kernel, we can increase the weighting of the kernel freely, achieving any variation desired. If a B_0 variation map is generated with a maximum variation of $100\mu T$ for instance, then this simply means that the multiplicative factor of our Gaussian kernel is $100E^6T$. This results in a map which is zero towards the center and approaches the value of $100\mu T$ towards the edges (figure 4.2). We will use the B_0 variation map from figure 4.2 to create a frequency shift in our standard slice selection. This is because the

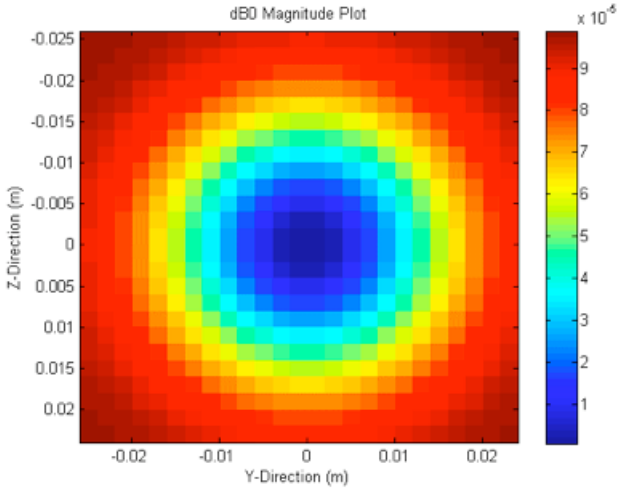

Figure 4.2.: B_0 variation map.

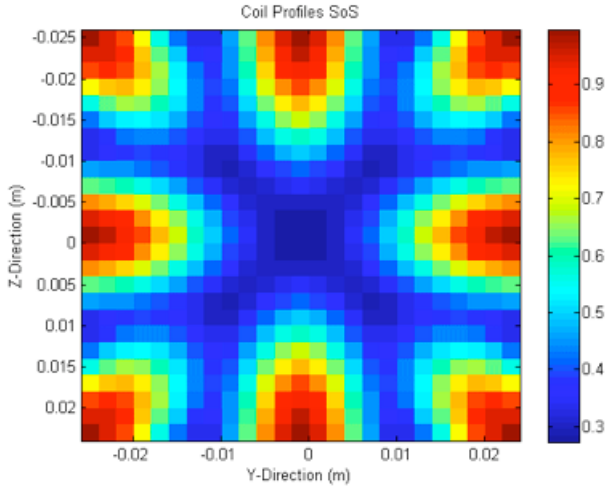

Figure 4.3.: Eight coils with Gaussian profile distributed around FOV (sum-of-squares representation).

local precessing frequencies of the spin-packets or isochromats change due to the variation in the local B_0 field:

$$\omega(x, z) = \gamma(B_0 + G_z(z) + \Delta B_0(x)). \tag{4.1}$$

Consider figure 4.3, which shows as an example an eight coil arrangement with their profiles combined using sum-of-squares (SoS). We will use the sensitivity information resulting from the coil profiles along with the main magnetic field inhomogeneity map to produce an aggregate excitation pattern which closely approximates the ideal excitation pattern. The target excitation pattern is estimated using the slice selection routine in the case where no inhomogeneity is present. By employing the

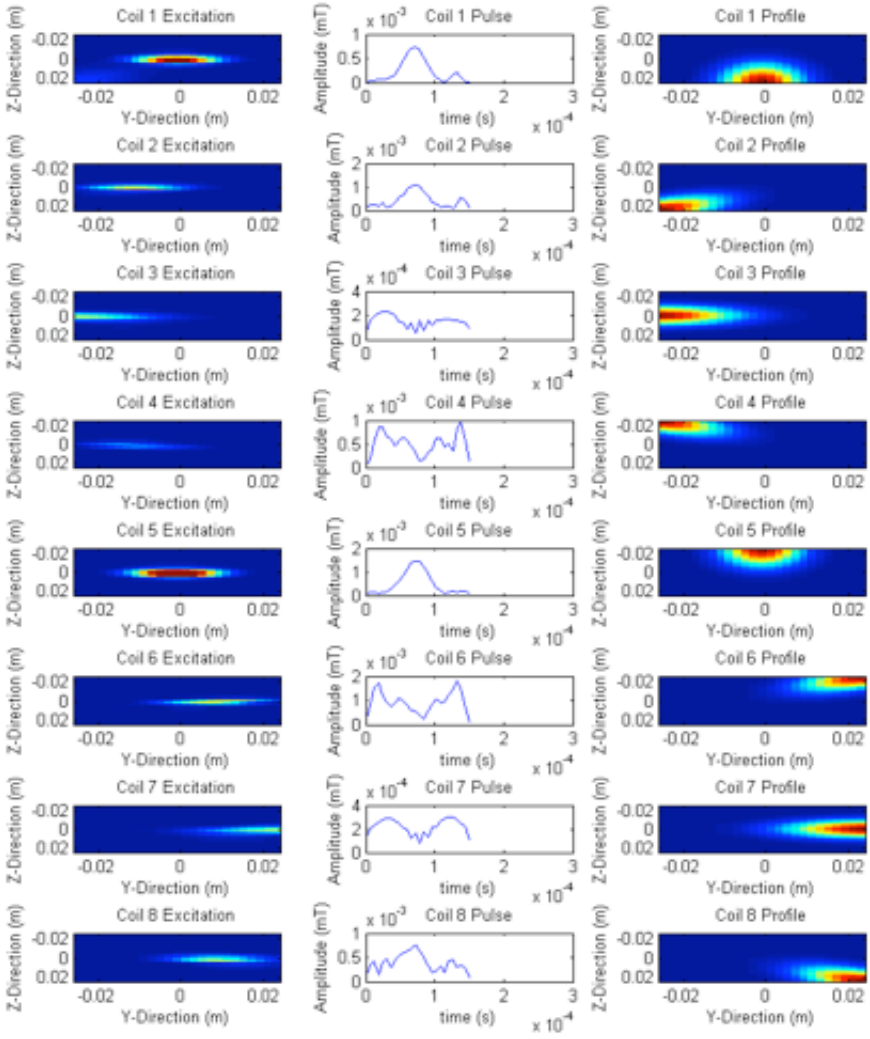

Figure 4.4.: Local excitation pattern and pulses for eight coil system using $100\mu T$ B_0 variation.

lsqr routine in MATLAB it is possible to invert the system encoding matrix. If we then multiply the target excitation pattern with the inverted matrix, we can acquire a set of ideal RF pulses. By then setting $\mathbf{m}_{actual} = \mathbf{A}_{full} \cdot \mathbf{b}_{opt}$ we obtain the actual aggregate excitation pattern. As can be seen in figure 4.4, depicting simulated data, the resulting excitation pattern from each coil is highly localized. Since some coils are either too far away from the target excitation pattern (coils 4 and 6), or because they are arranged in a way that does not help to offset the frequency variation (note we are only dealing with a single line of k-space in the y-direction, i.e. coils 3 and 7 cannot rectify the frequency offset, and their pulses are hence scaled down). Using the coil sensitivity information and our magnetic field model we can generate the inputs for the optimization. Figure 4.5(a) depicts the

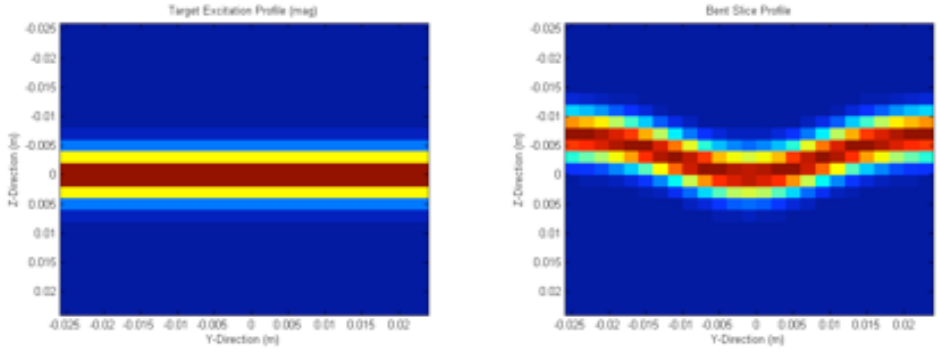

(a) Target excitation pattern. (b) Actual excitation pattern.

Figure 4.5.: Target Excitation and Resulting Slice Profile.

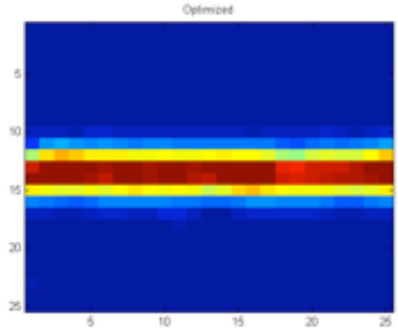

Figure 4.6.: Optimized aggregate excitation pattern (300 μT peak B_0 variation).

target slice excitation pattern, while figure 4.5(b) shows the actual slice excitation in the presence of B_0 inhomogeneity, which in this case has a peak value of $300\mu T$. Finally using $\mathbf{m}_{actual} = \mathbf{A}_{full} \cdot \mathbf{b}_{opt}$ we obtain the actual optimized aggregate excitation pattern (figure 4.6). Figure 4.7 shows an overview of the pulse played out on each coil (concatenated in a single vector as displayed in this figure), along with phase information and the target and actual excitation profiles. It is important to note that while this method does not have an implicit term for the frequency offset of each coil, it can achieve a desired change in frequency by virtue of a linear phase ramp.

4.3. Extended B_1-Shimming Method

This method is outlined as follows:

1. Definition of FOV in terms of frequency according to $\omega(x, z) = \gamma(B_0 + G_z(z) + \Delta B_0(x))$.

2. Generation of the target excitation pattern by setting ΔB_0 to zero.

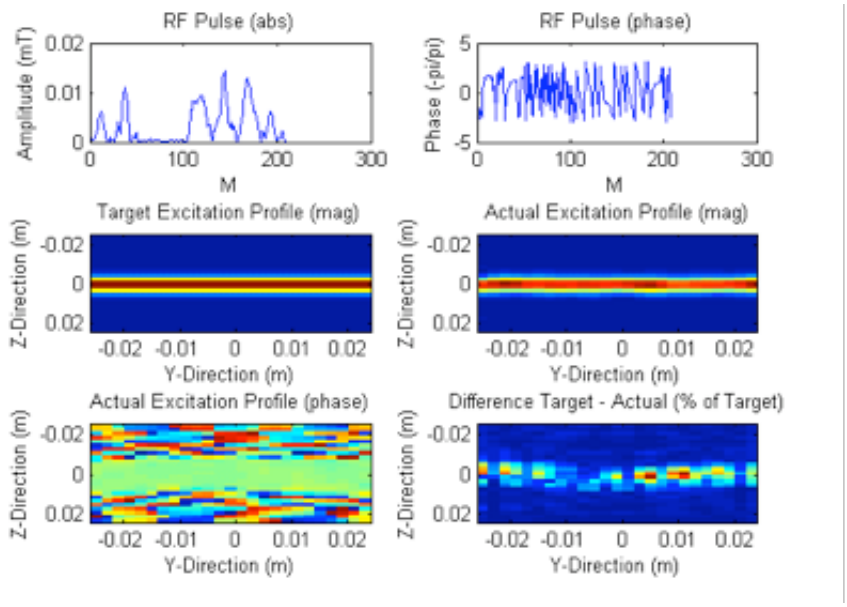

Figure 4.7.: Overview of the spatial domain method (300 μT peak B_0 variation).

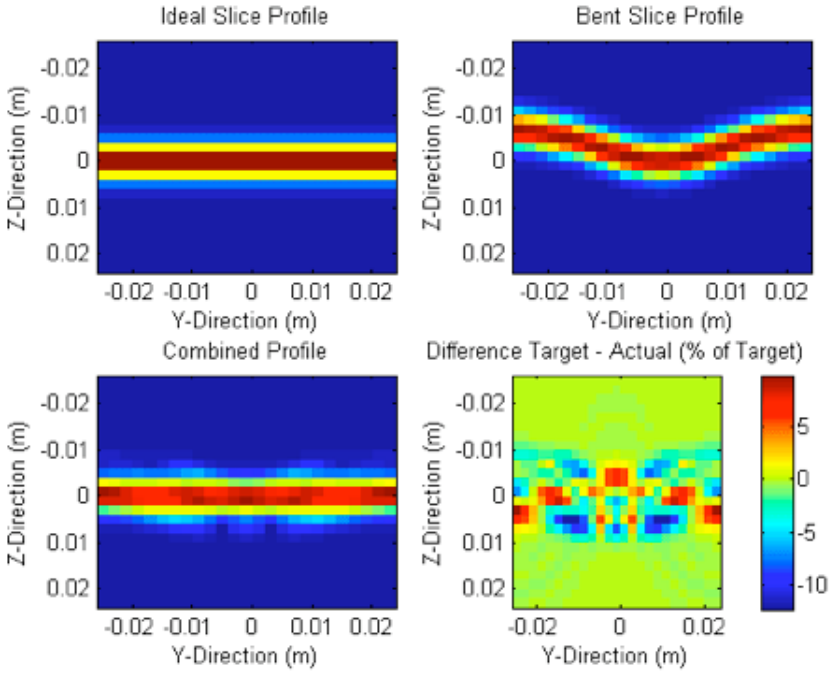

Figure 4.8.: Optimization results for B_1-Shimming Method (300 μT peak B_0 variation).

3. Generation of the actual excitation by including the main field in-homogeneity.

4. Optimization of center frequency, amplitude and global phase of the B_1 excitation profile for each coil.

As can be seen clockwise from the top-left in figure 4.8, first the ideal and bent slice profiles are generated. Then the combined actual excitation profile from a total of eight coils estimated alongside with the error expressed as a difference between the ideal and actual excitation as a percentage of the ideal excitation. The optimization routine concurrently derives weights for each of the twenty-four parameters that produce an optimal excitation profile.

4.4. Comparative Analysis

A comparison of the two established methods is presented in this section. Figures 4.9 and 4.10 show the result of the simulation of the slice correction algorithm for the Grissom and extended B_1 shimming method respectively. As mentioned previously in this chapter it is important to point out the explicit differences between the two established methods. The key point to note is that the extended B_1 shimming has three parameters per coil. This means that the dimensionality of the search space when compared to the Grissom method is greatly reduced. While a quick conclusion would be to say that because each point in the pulse can be optimized freely in the Grissom methodology it should therefore theoretically achieve better results since it has more parameters to play with. While this is true, and in general one would be able to say that the extended B_1 shimming method is merely a subset of the Grissom approach, it is important to note that having more parameters to control in an increased dimensional search space may lead to sub-optimal solutions. This can be attributed to what is known as the curse of dimensionality, meaning that a solution is prone to converge to a local minimum due to the increasing dimensionality of the search space. A more detailed look into this problem will be shown during the experimental verification.

4.5. Error Analysis

The Normalized Mean Square Error (NMSE), Normalized Root Mean Square Error (NRMSE) along with the peak, Mean Square (MS) and Root Mean Square (RMS) power are used to statistically describe the error for both the spatial domain and B1-shimming methods. The results of the experimental verification are expressed according to *fidelity* (NMSE, NRMSE) and *power* (Peak, MS, RMS). Note however that the fidelity and power measures are not estimated over the whole FOX but only around the area of the slice excitation, with its size being constrained by means of a simple thresholding function.

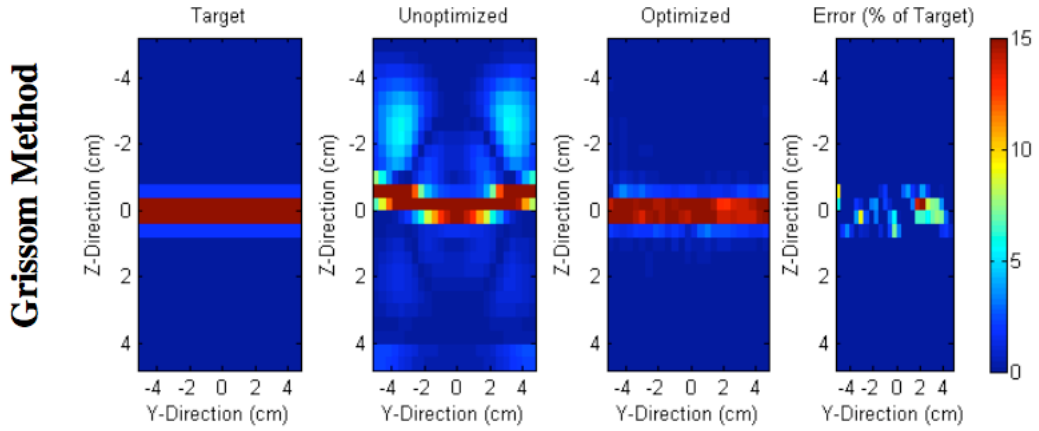

Figure 4.9.: Grissom method simulation (300 μT peak B_0 variation).

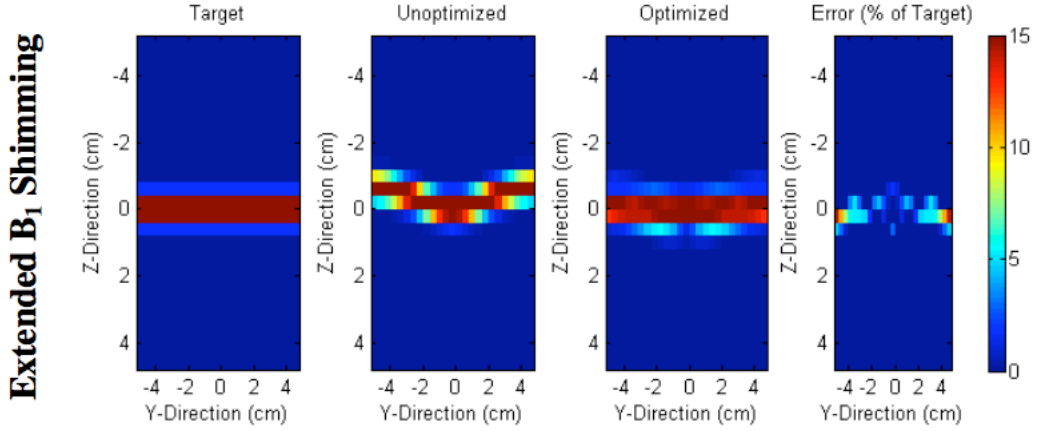

Figure 4.10.: Extended B_1 Shimming simulation (300 μT peak B_0 variation).

4.6. Hardware Setup

Two hardware setups are considered for this project. On the one hand there is the Philips 3T Multix system, from which field maps are obtained to support the simulation. On the other hand there is an experimental home-built system which can be used as a complement to an existing single channel scanner to achieve parallel excitation. This add-on system is built around a series of vector modulators, controlled by a computer, which can modulate the amplitude and phase of an incoming signal. The following section will present an overview over this experimental system.

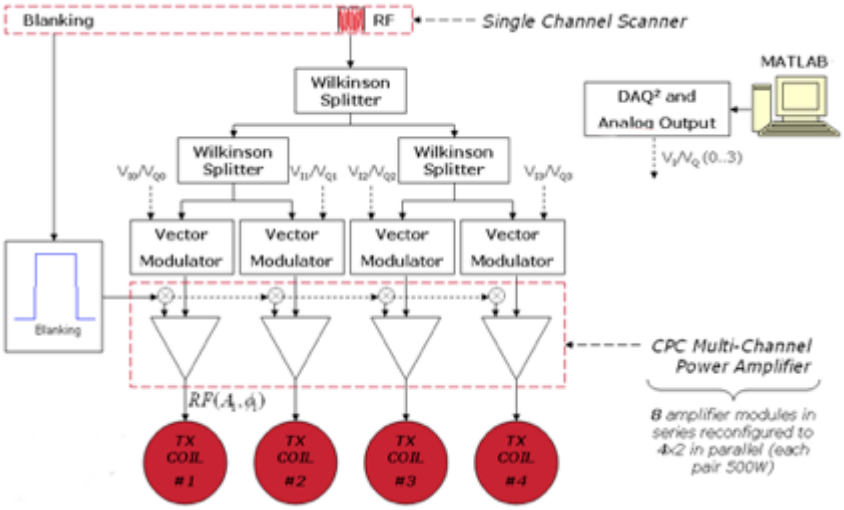

Figure 4.11.: Multi-Channel Architecture overview.

4.7. Experimental System

During the initial stages of the project a prototype PTx add-on system was built for the Philips 3T system. The aim was to create a parallel transmission architecture, which could be used to alter the Tx field, using a standard single transmit system as input. This was achieved by splitting the existing single transmit channel into multiple channels with independent control over the amplitude and phase. The add-on system was thus able to modulate the amplitude and phase for each individual channel. Using a Data Acquisition (DAQ) and Analog Output (AO) interface the amplitude and phase parameters can be controlled using a computer running MATLAB. Each channel is then amplified using a custom made multi-channel power amplifier supplied by Pulseteq Ltd. Because of the non-ideal behaviour of the various elements in the chain (figure 4.11) it is important to be able to account for inaccuracies and be able to calibrate the whole chain as quickly as possible. A mathematical model for the error was put in place and solved for the whole range of input values. This lead to a linear relationship between the expected output and the actual input data. The calibration of the system was turned into an automatic and autonomous routine employing a Network Analyzer to measure the actual output and MATLAB to provide a numerical estimate for the error and also account for it.

4.8. Results

The successful operation of one element of the aforementioned clinical add-on chain has been demonstrated. Since all four elements are identical it follows that if all

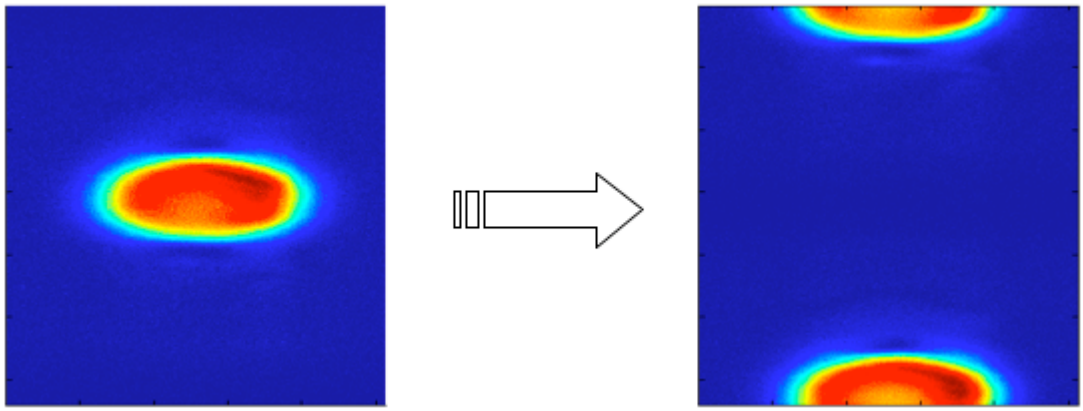

Figure 4.12.: Single-Loop coil under large phantom (left) with resulting $\frac{1}{2}$ FOV shift by alternating the phase between TRs (right).

the elements are combined, a whole operational system could be available. As depicted in figure 4.12, it can be seen that one vector modulator driving one of the home-made single loop coils can produce a provoked result. The aim of this experiment was to verify that if we alternate the phase (by 180°) between TRs, by using the control computer to synchronize with the scanner, it is possible to obtain a shift in the FOV without aliasing. As can be seen from the figure this proved to be correct and more elaborate testing using all four channels will provide evidence that the whole chain operates successfully. Another issue with the experimental vector modulator based chain is calibration, in order to account for the inaccuracies and nonlinearities introduced by the analog components such as the Wilkinson Splitters. For detailed results of this calibration please refer to [10].

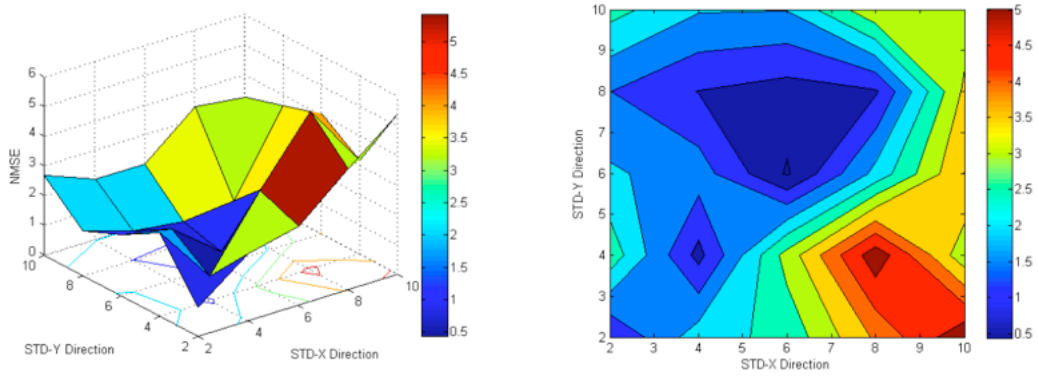

Figure 5.1.: Statistical evaluation of optimal coil size (300 μT peak B_0 variation).

5. Experimental Verification

Tests are carried out using synthetic and real coil data using a FOX of 0.1m x 0.1m with a resolution of 4 mm. The synthetic coils are placed in a circular arrangement around the FOX each having a Gaussian profile (figure 4.3). It is important to note at this point that the optimal coil size depends on the inhomogeneity of the magnetic field. The sizes for the synthetic coil data used for this simulation are statistically evaluated to yield the best results for a substantial amount of inhomogeneity introduced in the system. As can be seen from figure 5.1 the NMSE is plotted with respect to the size of the coil, expressed in terms of the standard deviation of the Gaussian profile in both x and y direction (i.e. height and width of the coil). The resulting optimal coil size is shown in the figure 5.2. The real coil data used, originating from the 3T Philips Multix system, is shown in the figures above (figures 5.3(a)-5.3(b)).

5.1. Synthetic Coil Data

We will start the experimental verification of the two implemented concepts by estimating fidelity and power measures for the synthetic coil data over a range of peak B_0 inhomogeneity values, ranging from 50 to 300 μT. From figure 5.4 we can see the NMSE plotted over a range of values for the main magnetic inhomogeneity. The NMSE increases smoothly as we increase the main magnetic field inhomogeneity. Even for a peak value of 300μT, for the respective methods, the error stays below

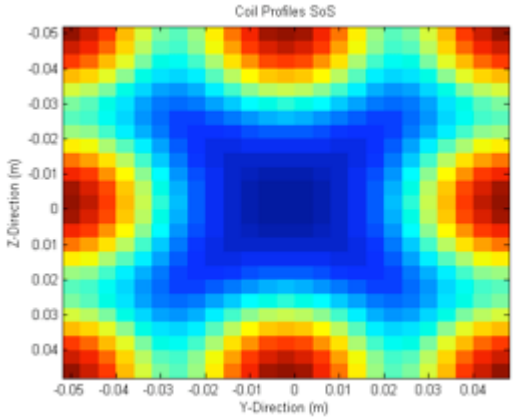

Figure 5.2.: Optimal coil size and profile for synthetic coil input data.

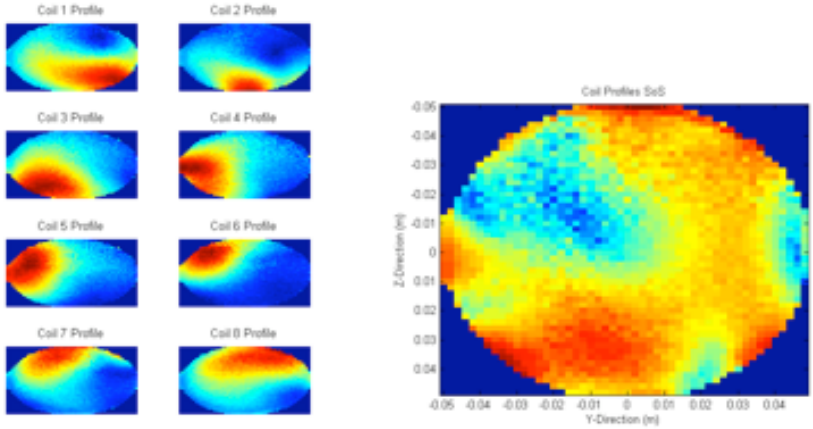

(a) Individual Coils for real coil data. (b) Sum-of-squares for real coil data.

Figure 5.3.: Overview of real coil profiles.

56% and 84% respectively; the results for the Grissom based method are shown in the left column and the B_1 shimming method in the right column. As expected the Grissom method outperforms the extended B_1 shimming method in terms of NMSE. The error of the B_1 shimming method is on average greater by a factor of 8.2 over the range plotted above. Figure 5.5 shows that the peak power follows a similar trend and scales up as we move towards a stronger main magnetic field distortion. This is something we would expect in theory; however it is important to note that compared to the baseline value for the peak power we can observe a substantial increase in transmitted power for both methods. The baseline or reference values are obtained by employing the same coil profile for each transmit coil. This single profile is the complex summation of all individual coils divided by the total number of coils. This way the same RF pulse is emitted from all coils and provides us with an, albeit heavily underestimated, reference value. A full list of

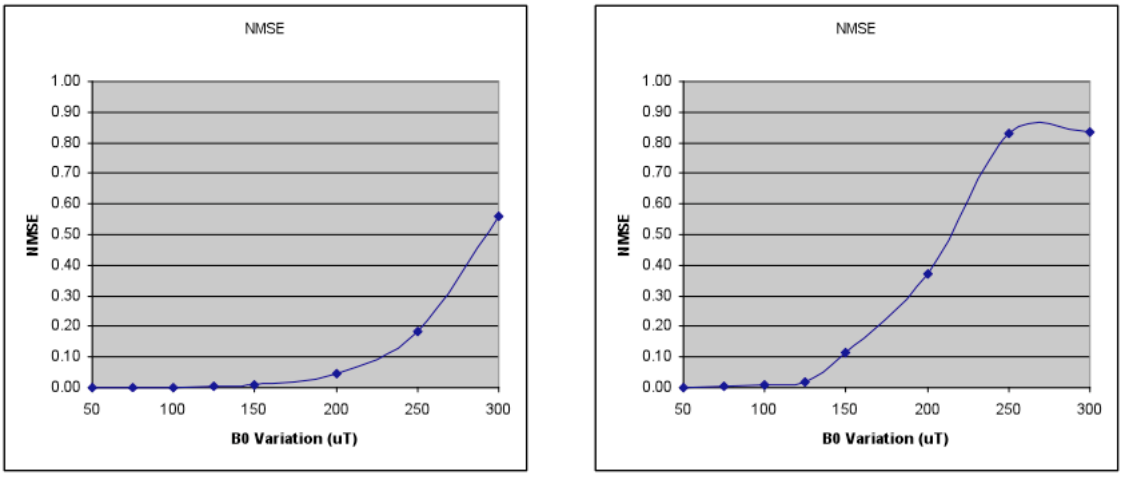

Figure 5.4.: Fidelity comparison using synthetic coil data.

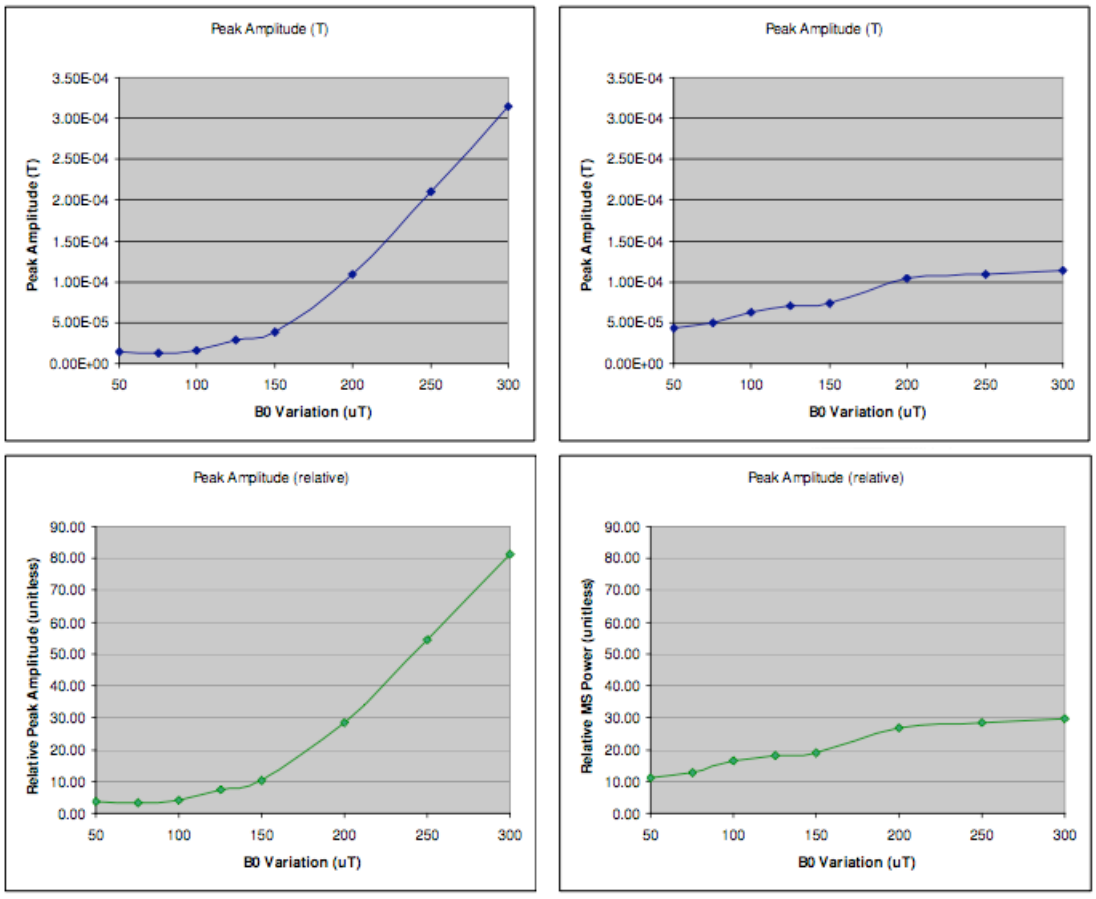

Figure 5.5.: Power comparison using synthetic coil data.

the reference values and the obtained results can be found in the appendix. For a peak variation of 50 μT the peak value of any coil using the Grissom method

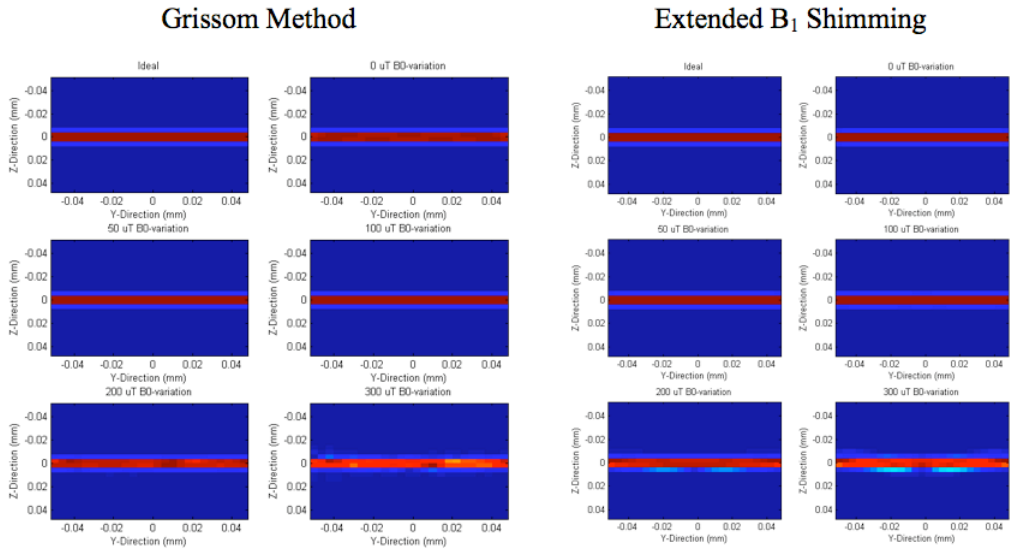

Figure 5.6.: Overview of resulting profiles over a range of ΔB_0 (0-300 μT) values using synthetic coil data.

is around 14 μT while for the extended B_1 shimming method it is around 43 μT. For this degree of inhomogeneity the respective MS power values are 8 μT^2 and 507 μT^2 for each method respectively. On average the MS power of the extended B_1 shimming method is greater by a factor of 50 when compared to the Grissom method. However note that the power in the extended B_1 shimming method, as exemplified by the graph for the peak amplitude in the table above, does not scale up in the same way as in the Grissom approach. In the Grissom approach the power scales up in a quasi quadratic fashion as it tries to find an optimal solution for an ever growing distortion of the main magnetic field. The extended B_1 shimming approach is intrinsically less well conditioned in terms of power and therefore starts off with much higher power when compared to the estimated baseline. However for extreme distortions of the main magnetic field of 200 μT and above this method does not increase the power as strongly as the Grissom approach. This can be due to numerous factors which will be enumerated at the end of this chapter.

Figure 5.6 shows the resulting excitation profile over a range of different main field inhomogeneities for both methods; the results for the Grissom based method are shown in the left column and the B_1 shimming method in the right column. Visually even for high variations (50 μT 200 μT) over such a small field of view the results can be deemed acceptable. Using synthetic coils in our simulation we can observe that both methods produce satisfactory results. With respect to the fidelity measures both methods follow a similar pattern and the error scales up as

we introduce more distortion into the system. In terms of power the extended B_1 shimming method exceeds the baseline-values on average by a greater factor than the Grissom method.

5.2. Real Coil Data

In addition to using synthetic coil data, we will evaluate the fidelity and power measures using real coil maps. The results for the spatial domain method are presented alongside the results of the B_1-shimming method. As can be seen from figure 5.7, in terms of fidelity, the B_1-shimming method outperforms the spatial domain method. This is due to the fact that, for one part, the coil data is noisy and not well localized, but also because the power scaling is more realistically constrained in the spatial domain method. This means that essentially the solution space of the real coil data is more complex than for the synthetic coil data. Consequently the solution using the Grissom method converges towards a non optimal local minimum because of the bigger parameter space of this method and the more complex solution space of this coil data. The average NMSE of the Grissom method is bigger by a factor of 2.5 when compared to the extended B_1 shimming method. However note that the average peak power of the extended B_1 shimming method is greater by a factor of 115 when compared to the Grissom method. Compared to the baseline values only the Grissom method stays within reasonable limits as the extended B_1 shimming method substantially overshoots the baseline reference. The important point to note from this analysis is that while the Grissom method offers more flexibility or degrees of freedom, it is also more likely to get trapped in non optimal solutions. Using real coil data, which is more complex than modelled coil profiles, we can see a major shortcoming of the Grissom method. Theoretically the Grissom method should outperform the extended B_1 shimming method, however in the current implementation this is not the case. There are various improvements which can be made to the Grissom method to make it more robust in an increasingly complex search space, and will be briefly addressed in the concluding section of this chapter. Figure 5.8 shows the resulting excitation profile over a range of different main field inhomogeneities for both methods. We can see that the Grissom method breaks up quickly because the optimization process is caught in a non optimal local minimum. The results for the extended B_1 shimming method however produce quite impressive visual results even for extreme main field distortions.

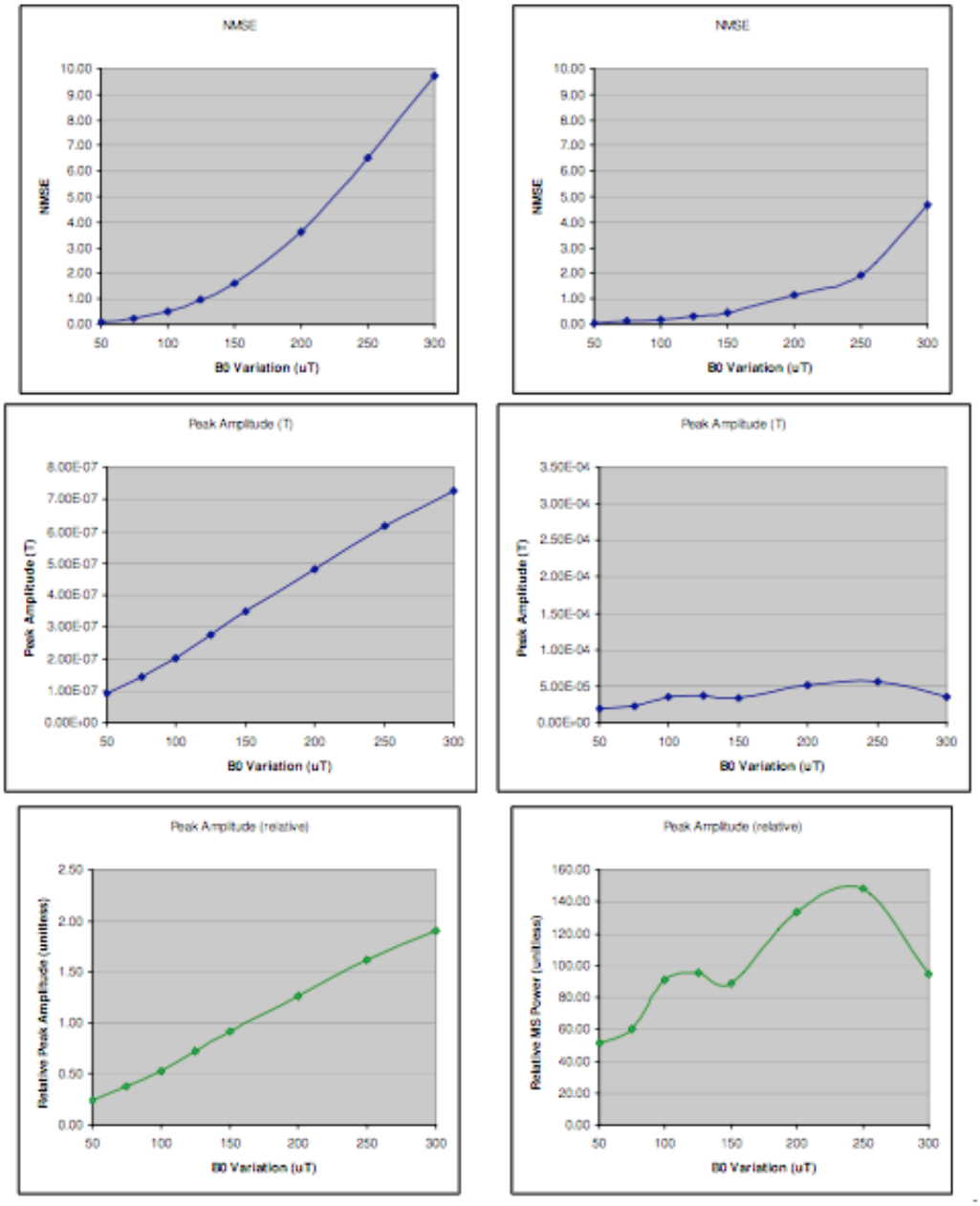

Figure 5.7.: Fidelity and power comparison using real coil data.

5.3. Conclusion

We have presented and experimentally evaluated two distinct methods to address the problem of correcting a bent slice during an MR experiment. They are based on concepts established in the area of parallel transmission. We have seen that these methods essentially differ in the amount of parameters they control. Both methods can account for externally induced main magnetic field inhomogeneities, even at

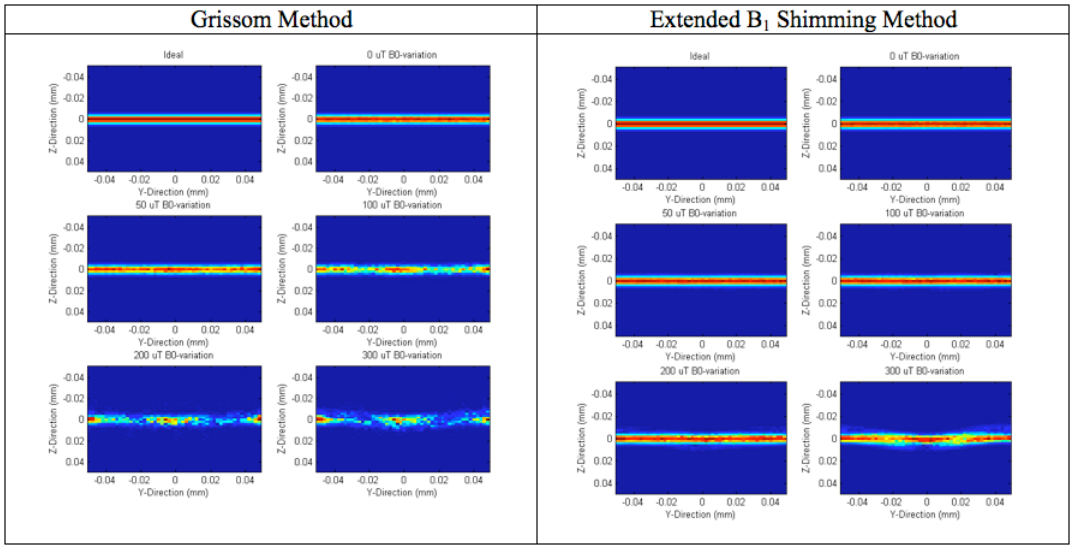

Figure 5.8.: Overview of resulting profiles over a range of ΔB_0 (0-300 μT) values using real coil data.

extreme levels. Due to the limitations of this simulation we have also seen that both methods are prone to converge to non optimal solutions and therefore only provide an indication as to what would be possible to achieve in the real world. The results obtained however suggest that both methods could be implemented and tested on a clinical scanner in order to address the problem of a bent slice. The methodology on which the Grissom approach is based can be implemented directly on the Philips 3T Multix system, however this is beyond the scope of this project. Using the add-on hardware, as refined during the course of this project, it is possible to implement the extended B_1 shimming method on virtually any standard MRI scanner. In order to make this implementation more robust there are a few things to consider. On the one hand the optimization routine should include multiple passes through the data-space to reduce the likelihood of reaching a local minimum. On the other hand the estimation of the cost function should be improved to include more constraints and regularization. As a subsequent step it would be desirable to produce an implementation of the concepts outlined in this report on a clinical MRI system, such as the Philips Multix system, as we showed that the slice correction method works.

A. Appendix

Table A.1.: Baseline Values.

	Synthetic Coil Data	Real Coil Data
Peak (T)	3.87E-06	3.81E-07
MS	1.20E-09	1.09E-07
RMS	2.40E-06	6.42E-09

Table A.2.: Spatial Domain Method (Synthetic Coil Data).

ΔB_0 (μT)	50	75	100	125	150	200	250	300
NMSE	1.44E-04	3.04E-04	1.30E-03	3.80E-03	8.80E-03	4.51E-02	1.84E-01	5.61E-01
NRMSE	1.20E-03	1.70E-03	3.60E-03	6.10E-03	9.40E-03	2.12E-02	4.29E-02	7.49E-02
Peak (T)	1.39E-05	1.25E-05	1.55E-05	2.81E-05	3.93E-05	1.10E-04	2.11E-04	3.15E-04
MS	8.00E-06	4.90E-06	7.80E-06	1.64E-05	3.08E-05	1.92E-04	5.95E-04	1.13E-03
RMS	6.20E-06	4.90E-06	6.10E-06	8.90E-06	1.22E-05	3.03E-05	5.35E-05	7.36E-05

Table A.3.: Spatial Domain Method (Real Coil Data).

ΔB_0 (μT)	50	75	100	125	150	200	250	300
NMSE	7.89E-02	2.31E-01	5.21E-01	9.67E-01	1.61	3.62	6.50	9.72
NRMSE	2.81E-02	4.81E-02	7.22E-02	9.83E-02	1.27E-01	1.90E-01	2.55E-01	3.12E-01
Peak (T)	9.12E-08	1.43E-07	2.02E-07	2.74E-07	3.50E-07	4.81E-07	6.18E-07	7.26E-07
MS	2.46E-10	5.58E-10	1.08E-09	1.90E-09	3.07E-09	6.34E-09	1.06E-08	1.52E-08
RMS	1.09E-09	1.64E-09	2.27E-09	3.02E-09	3.84E-09	5.52E-09	7.15E-09	8.55E-09

Table A.4.: B_1-Shimming Method (Synthetic Coil Data).

ΔB_0 (μT)	50	75	100	125	150	200	250	300
NMSE	2.20E-03	3.50E-03	9.00E-03	1.95E-02	1.16E-01	3.70E-01	8.31E-01	8.36E-01
NRMSE	4.70E-03	5.90E-03	9.50E-03	1.40E-02	3.41E-02	6.08E-02	9.12E-02	9.14E-02
Peak (T)	4.29E-05	4.93E-05	6.33E-05	7.09E-05	7.40E-05	1.04E-04	1.09E-04	1.14E-04
MS	5.07E-04	7.01E-04	1.12E-03	9.96E-04	1.08E-03	2.39E-03	2.44E-03	2.85E-03
RMS	1.38E-05	1.63E-05	2.06E-05	1.94E-05	2.02E-05	3.00E-05	3.04E-05	3.28E-05

Table A.5.: B_1-Shimming Method (Real Coil Data).

ΔB_0 (μT)	50	75	100	125	150	200	250	300
NMSE	5.41E-02	1.33E-01	1.80E-01	3.28E-01	4.76E-01	1.13	1.95	4.66
NRMSE	2.33E-02	3.64E-02	4.24E-02	5.72E-02	6.90E-02	1.06E-01	1.40E-01	2.16E-01
Peak (T)	1.95E-05	2.31E-05	3.46E-05	3.63E-05	3.38E-05	5.08E-05	5.65E-05	3.60E-05
MS	8.81E-05	1.27E-04	2.10E-04	2.45E-04	2.93E-04	5.15E-04	6.83E-04	3.12E-04
RMS	1.82E-07	2.19E-07	2.81E-07	3.04E-07	3.32E-07	4.41E-07	5.08E-07	3.43E-07

Bibliography

[1] Liang Z-P, Lauterbur P C, "Principles of Magnetic Resonance Imaging - A Signal Processing Perspective", IEEE Press Series in Biomedical Engineering, 2000.

[2] Lustig M, Donoho D, Pauly JM, 2007. Sparse MRI: The Application of Compressed Sensing for Rapid MR Imaging. Magnetic Resonance in Medicine 58, 1182-1195.

[3] Tsao J, Boesiger P, Pruessmann K P, 2003. k-t BLAST and k-t SENSE: Dynamic MRI with High Frame Rate Exploiting Spatiotemporal Correlations. Magnetic Resonance in Medicine 50, 1031-1042.

[4] Katscher U, Bornert P, 2006. Parallel RF Transmission in MRI. NMR in Biomedicine 19, 393-400.

[5] Pruessmann K P, Weiger M, Scheidegger M B, Boesiger P, 1999. SENSE: sensitivity encoding for fast MRI. Magnetic Resonance in Medicine 42, 952-962.

[6] Zhu Y, 2004, Parallel Excitation With an Array of Transmit Coils. Magnetic Resonance in Medicine 51, 775-784.

[7] Katscher U, Bornert P, Leusseler C, van den Brink JS, 2003. Transmit SENSE. Magnetic Resonance in Medicine 49, 144-150.

[8] Setsompop K, Wald L L, Wijayanand A, Gagoski B, Hebrank F, Fontius U, Schmitt F, Adalsteinsson E, 2006, Parallel RF Transmission With Eight Channels at 3 Tesla. Magnetic Resonance in Medicine 56, 1163-1171.

[9] Grissom W, Yip C-y, Zhang Z, Stenger A, Fessler J A, Noll D C, 2006, Spatial Domain Method for the Design of RF Pulses in Multicoil Parallel Excitation, Magnetic Resonance in Medicine 56, 620-629.

[10] Filos J, Malik S, Randall C, Cooper M, Herlihy D, Larkman DJ, Hajnal JV, "A Parallel Transmit System for Single Channel Scanners", 2008, 17th Annual NMR Symposium, Sheffield.